Georg-August-Universität Göttingen

Geowissenschaftliches Zentrum Göttingen

Modelling the influence of thermal springs in fault zones on subsurface temperature in the Alps

Master Thesis

by

Saskia Köhler

From Kerpen, Germany

29.01.2019

Supervisor: Dr. Elco Luijendijk, Department of Structural Geology and Geodynamics, Georg-August-Universität, Göttingen, Germany

Co-supervisor: Dr. Christoph von Hagke, Energy and Mineral Resources Group, Rheinisch-Westfälische Technische Hochschule, Aachen, Germany

Tabel of contents

Table of figures

Zusammenfassung

Temperaturen des Untergrundes und der Gesamtwärmegehalt sind maßgebliche Komponenten in gebirgsbildenden Prozessen, sowie bei der Interpretation von thermochronologischen Daten. Der thermische Effekt von Grundwasserfluss auf den Wärmehaushalt aktiver Orogene ist bisher nicht quantifiziert worden. Ich nutze eine Zusammenstellung vorhandener Daten thermaler Quellen in den europäischen Alpen, um den Beitrag der Quellen zu dem gesamten Wärmehaushalt des Orogens zu analysieren. Des Weiteren präsentiere ich ein detailliertes numerisches Modell, das die thermische Entwicklung der hydrothermalen Quellen in Bormio (Italien) und den Einfluss von Fluidfluss auf die Temperatur im Untergrund simuliert. Die Ergebnisse zeigen einen Anteil von bis zu 1.3 % des Fluidflusses auf den gesamten Wärmefluss der Alpen. Das Fallbeispiel des Quellsystems in Bormio zeigt, dass die Quelltemperaturen nach 100 bis 350 Jahren Gleichgewichtszustand erreichen. Das aufströmende Wasser beeinflusst die Untergrundtemperaturen in einem Radius von 430 m. Sensitivitätsanalysen zeigen einen starken Effekt des geothermischen Gradienten, des Fluidfluss entlang der Störung und der Störungstiefe auf die Quell- und Untergrundtemperaturen. Die Quantifizierung des Beitrags von Grundwasserfluss zum thermischen Feld stellt neue Grenzen für die Interpretation thermochronologischer Daten dar. Die Simulation der Entwicklung des Quellsystems in Bormio bringt neue Erkenntnisse zu der Beständigkeit hydrothermaler Quellen im Verlaufe der Zeit.

Abstract

Subsurface temperature and heat budget are key components in mountain building processes and important for the interpretation of thermochronological data. However, the thermal effect of groundwater flow on the heat budget of active orogens remains unquantified. I used a compilation of thermal spring data in the European Alps to analyse the contribution of thermal springs to the overall heat budget of the orogen. In addition, I present a detailed numerical model which simulates the thermal history of the Bormio hydrothermal spring system (Italy) and the influence of fluid flow on subsurface temperature in a fault zone. The results show that fluid flow contributes up to 1.3 % of the total heat flow in the Alps. The case study of the Bormio spring system shows that spring temperatures reach a steady-state after 100 to 350 years. The up flowing water affects subsurface temperatures in an area with a radius of 430 m. Performed sensitivity analysis show a strong effect of the geothermal gradient, fluid flow across the fault and fault depth on spring temperature. The quantification of the contribution of groundwater flow to the thermal fields provides new constrains on the interpretation of thermochronological data. The simulation of the thermal history of the Bormio spring system provides new insights on the persistence of thermal springs over time.

1. Introduction

Temperatures and heat budget are key parameters influencing rock rheology and thus contribute to mountain building processes. Temperature and heat flow are key constraints for geodynamic models of the lithosphere (Artemieva et al., 2006). Furthermore, knowledge of the timing and rate of exhumation of orogens is largely based on the interpretation of thermochronological data (Reiners and Brandon, 2006). The interpretation of such thermochronological data relies on subsurface temperatures. Hydrothermal activity can effect these datasets (Louis et al., 2018; McInnes et al., 2005). Subsurface temperature data is rare in the Alps, with less than 600 measured heat flow data points in the entire Alps (Hasterok, in prep.). Thermal springs are outcrops for deep fluid flow and heat transport in orogens. Therefore, I supplemented the information about the thermal field gained from the global heat flow database (Hasterok, in prep.) with temperature and flow rate data from thermal springs. Fractures and vertical strata are consequences of folding and faulting due to subduction and collision events. This favours upwelling of deep ground water and makes thermal springs relative abundant in orogens (Ferguson and Grasby, 2011). The subsurface gets cooled by the heating of infiltrating cold meteoric water, which discharges through springs again. Therefore, the earth is losing heat by water circulation. In some regions models and data show that fluid flow causes up to 50 % of the overall heat transport (Derry et al., 2009; Ferguson and Grasby, 2011; Grasby and Hutcheon, 2001; Ingebritsen et al., 1992; Whipp and Ehlers, 2007). This heat loss due to the discharge of warm water and its effect on the thermal field of orogens has not been quantified systematically, yet. The European Alps have more than 400 springs with temperatures of up to 71 °C (fig. 1). Based on a database containing temperature data and flow rates of the thermal springs I quantified the contribution of thermal springs to the heat budget of the overall orogen. In addition, I evaluated the distribution of thermal springs over the orogen considering lithology, fault systems and elevation.

In the second part of this work I will present a numerical model. Because of the lack in available data for temperature and heat flow in the subsurface I simulated the subsurface temperature under consideration of thermal spring data. I selected the thermal spring system of Bormio (Italian Alps) with discharge temperatures up to 43 °C for a more detailed analysis of the influence of fault properties on the temperatures of the spring water and to the subsurface temperatures over time. This model is used to quantify the correlation between water circulation and the thermal field in fault zones.

2. Geological setting

2.1 Alps

I studied the heat flow and the distribution of thermal springs in the entire European Alps. The Alps result from two distinct mountain building phases, the Eo-Alpine orogeny in the Jurassic, and the Tertiary Alpine collision. The Alps are tectonically subdivided into Helvetic, Penninic, Austro-Alpine and South Alpine units (Froitzheim et al., 2008). The tectonic and morphologic boundary between the Southern Alps to the other units is defined by the Neogene E-W trending Periadriatic Line. The Periadriatic Line is well visible in the alpine topography as a series of adjacent valleys (e.g. Gailtal, Valtellina Valley). North of the Periadriatic Line the nappe system consist of the Helvetic units at the base, overlaid by the Penninic units and the Austro-Alpine units (Froitzheim et al., 2008). The Austro-Alpine and the South Alpine units consist of Apulian continental crust, whereas the Helvetic nappes consist of European crust and the Penninic units of oceanic crust (Froitzheim et al., 2008). On maps the Apulian parts are separated from the European and oceanic parts by the Periadriatic Line and by a N-S trending suture running from Lake Constance to the south. The development of the Alps in two phases causes sets of faults and folds that can roughly be classified into these two ages (Conti et al., 1994; Froitzheim et al., 2008). Due to the present counter clockwise rotation of the Adriatic microplate a convergence rate between 2 and 3 mm year^{-1} is measured in the southern Alps (Calais et al., 2002; D'Agostino et al., 2005; DeMets C. et al., 1990) whereas in the Western Alps the dominating regime is extensional (Calais et al., 2002). Furthermore, the Alps are uplifting with rates of up to 1.5 mm year^{-1} (Schlatter et al., 2005). This is caused by crustal thickening as a consequence of the convergence. In addition, the load of the ice shields during the last glaciation caused the Alps to be pushed deeper into the lithosphere. This glacial period ended around 11000 – 12000 years ago (Hormes et al., 2008), causing deglaciation and present day isostatic uplift. The neotectonic activity in the Alps is also represented by seismicity (Arcoraci et al., 2012; Husen et al., 2007; Ustaszewski and Pfiffner, 2008).

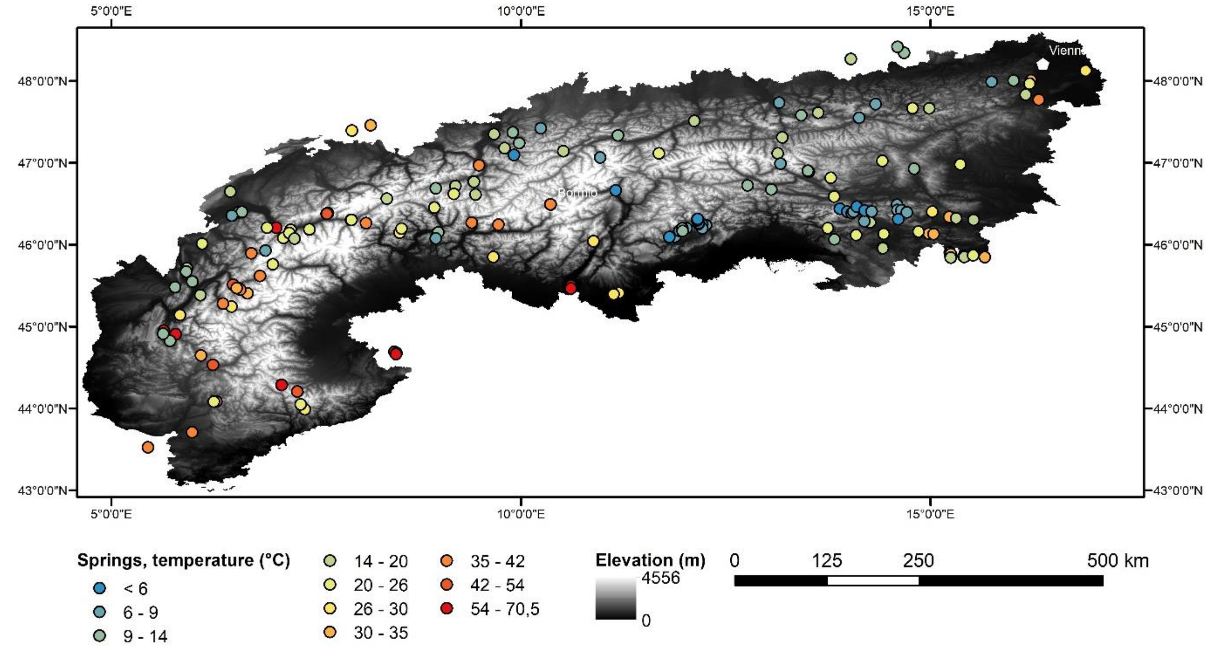

Figure 1: The elevation map of the Alps, the location of thermal springs and their discharge temperatures (°C). Elevation from Danielson and Gesch (2011)

2.2 Bormio

To quantify the influence of fluid flow on the subsurface temperature over time I performed a detailed numerical simulation. I have chosen the thermal spring system of Bormio which has been known and used since Roman times. The regional geology has been described by Conti et al. (1994) and Froitzheim et al. (1994 and 1997) and the hydrological setting by Volpi et al. (2017). These previous works provide a lot of valuable data which is used in this work and which make the results comparable.

Bormio is located in the Italian Alps, on the southern boundary of the Engadine Dolomites, in the Upper east-west orientated Valtellina Valley (Froitzheim et al., 2008). The city of Bormio is south of the Zebrù Thrust system on the metapelites of the Campo Nappe. They are partially covered by quaternary alluvial fans (fig. 2). The Zebrù Thrust is of Cretaceous age and defines the contact between the Paleozoic Campo Nappe in the south and the Triassic Ortler Nappe in the north (fig. 2) (Conti et al., 1994; Froitzheim et al., 1994). The fault is E-W trending and dips at approximately 60 ° to the north. Both nappes belong to the Austro-Alpine units (Froitzheim et al., 1997). The Ortler Nappe consists of dolomite and limestone. The Trupchun-Braulio Thrust crops out approximately 4 km further up north, being of the same age and direction as the Zebrù Thrust. Another 7 km towards the north the S-dipping Gallo Line occurs. This is a Cretaceous normal fault that separates the S-charl-Sevanna Nappe in the north from the Quattervals Nappe in the south (Froitzheim et al., 1994). It is unclear if this fault is connected to the Zebrù and Trupchun-Braulio thrusts at depth (Froitzheim et al., 1994, 1997). 30 km to the south runs the Neogene Periadriatic Line.

Ten springs with discharge temperatures in the range of 18 - 43 °C and flow rates up to 0.02 $m^3\ s^{-1}$ are located close to the Zebrù Thrust (fig. 2). The mean flow rate is 0.004 $m^3\ s^{-1}$. In sum the system provides a fluid rate of 0.04 $m^3\ s^{-1}$. All of the springs discharge in the dolomites of the hanging wall in the north. According to Volpi et al. (2017), who measured δ^2H and $\delta^{18}O$ isotopes, recharge of meteoric water is assumed to originate from above the Passo del Stelvio (Volpi et al., 2017) at an elevation of around 3000 m.a.s.l. (meters above sea level) and peaks up to 3700 m.a.s.l. (Thurwieserspitze).

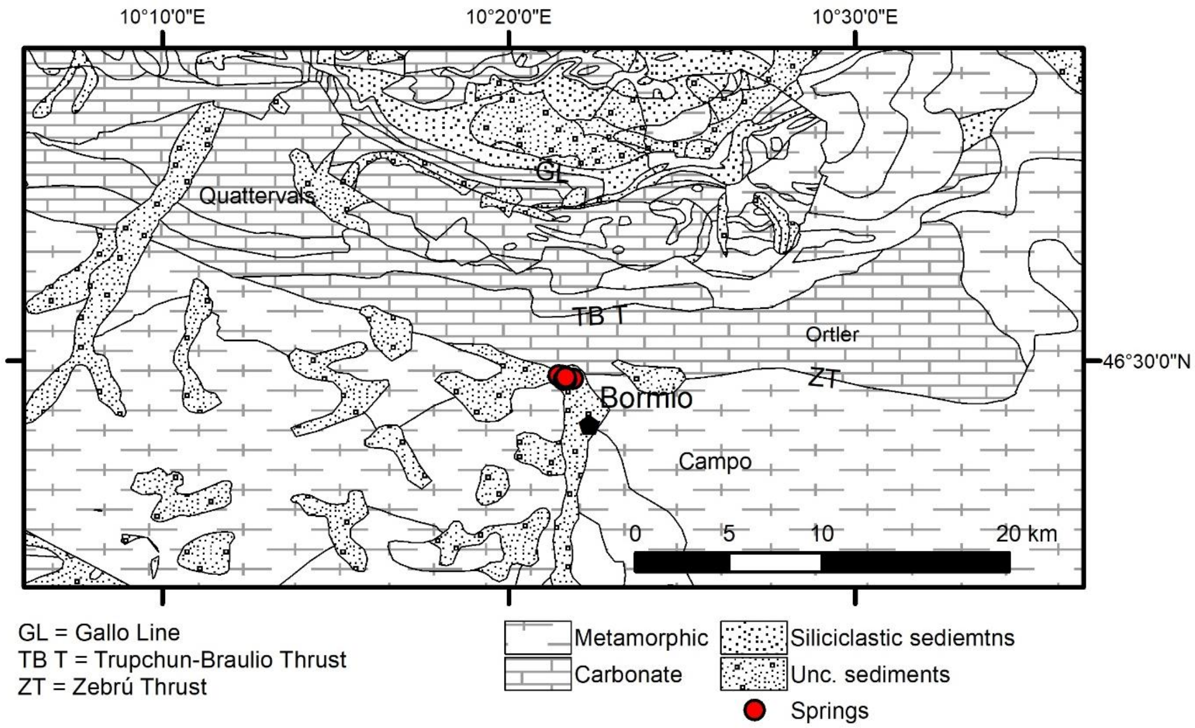

Figure 2*:* A geological map showing the location of the Bormio springs south of the Zebrù Thrust (ZT). Lithology from Hartmann and Moosdorf (2012).

3. Material and Methods

3.1 Thermal spring database

For all springs I used our new database of approximately 800 springs, boreholes and tunnels. The data includes location and altitude. Discharge temperature and flow rate are provided for 550 springs. For boreholes, the depth is included as well. If a spring is associated with faults we compiled published data on angle, depth and age of the fault. The database contains lithological data of the rocks hosting springs and hydrochemical and isotopic data of the spring water. Most of this data is collected by literature research. For example, we used measurements from Kanduč et al.(2012). They measured flow rates, temperatures, chemical and isotopic data for twelve springs in the Slovenian Alps. The complete data set is included in the electronic supplement. Because the database contains springs that are located outside of the defined boundaries of the Alps (ESDAC), I considered only 234 of the springs in this work. In addition, I used existing databases. The Laboratoire de géothermie for example provides a list of information on most Swiss springs (CREGE). For fault locations I used databases of national surveys, like the LGRB (Landesamt für Geologie, Rohstoffe und Bergbau) for the German Alps and GBA (Geologische Bundesanstalt) for Austria. Data on the location of faults are not available for the entire Alps (fig. 4). However, a shape file for the global surface geology is provided by Hartmann and Moosdorf (2012). In this work I used geological data for the entire orogen. I also used the Global Heat Flow Database from Hasterok (in preparation), which contains surface heat flow data and geothermal gradients from 12000 boreholes worldwide of which 596 are from the Alps.

3.2 Heat contribution of thermal springs

To calculate the heat contribution of the springs I used only those springs which provide both temperature and flow rate data and which are inside of the defined boundaries. The area of the Alps was defined by a shape file offered from the ESDAC (European Soil Data Centre). Thus, I calculated the heat contribution of 234 considered springs as:

$$\mathrm{HF} = \Delta T \; Q \; \rho \; c_{P},_{f} \tag{1}$$

where HF is heat flow (W), ΔT is the difference between recharge and discharge temperature (K), Q is the flow rate at the spring ($m^3 s^{-1}$), ρ is density ($kg\ m^{-3}$) and $c_{p,\ f}$ is heat capacity of water and of the surrounding rock ($J\ kg^{-1}\ K^{-1}$).

To simplify the model, I used a constant density of 1000 $kg\ m^{-3}$ for water with a heat capacity c_f of 4000 $J\ kg^{-1}\ K^{-1}$ and a constant heat capacity c_p of 900 $J\ kg^{-1} K^{-1}$ for the surrounding rock.

I set the recharge temperature equal to the average air temperature (T_{air}). Following Rolland (2003), T_{air} depends on latitude and altitude and is unknown for the spring locations. Therefore, I needed to calculate the relation between these two parameters using a reference temperature ($T_{reference}$) at sea level to quantify the recharge temperature. $T_{reference}$ is given by eq. 2 with an average lapse rate a of −0.56 °C (100 m)$^{-1}$ (Rolland, 2003).

$$T_{\text{reference}} = T_{\text{air}} - \mathrm{a} \times z \quad (2)$$

Altitude (z) is given in m. I used annual average temperatures (°C) measured over 30 years from weather stations by the DWD (Deutscher Wetterdienst) with known latitude and altitude. The relation between $T_{reference}$ (°C) and the latitude shown in fig. 3 is calculated using linear regression.

$$T_{\text{air}} = m \times \text{lat} + c \quad (3)$$

I calculated the size of the area A (m²) that contributes recharge for each spring:

$$A = Q/R \quad (4)$$

Q denotes the flow rate at the spring (m³ s^{-1}) and R is the recharge rate (m s^{-1}). Here I used the recharge rate from the global recharge database by de Graaf et al. (2017). For simplification I assume A to be a circle. The doubled radius of the circle is then the distance between the spring at the minimum and the edge of the recharge area at the maximum elevation. I did this simplification because I do not have knowledge about the regional hydrology for the entire Alps. Elevation was obtained by the digital elevation model (DEM) GMTED2010 (Danielson and Gesch, 2011). I used slope m and y-axis intercept c from the regression (fig. 3) to calculate T_{air} (°C) for each spring (eq. 3). Using these values for eq. 1, I get the minimum and maximum heat flow for each single spring. The sum of these is a first estimate for the advective heat flow by groundwater in the Alps.

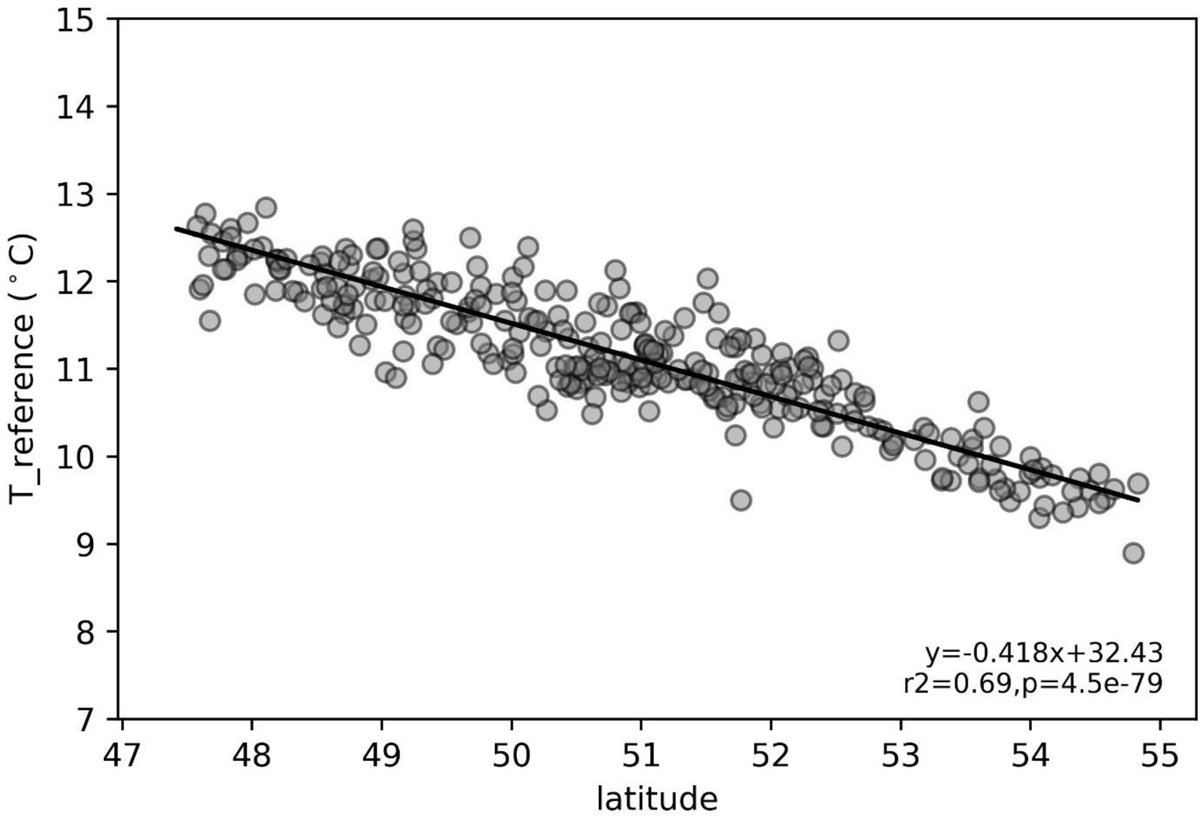

Figure 3: Relation between latitude and the reference temperature at sea level which was calculated with equation 2, by Rolland (2003) based on measurements by the DWD.

3.3 Statistic evaluation

For statistics I used the database mentioned in section 3.1 as well as secondary databases containing lithology from Hartmann and Moosdorf (2011) and fault data by the LBRG and the GBA. I compared the springs to 1000 points distributed randomly over the Alps. I calculated the relief of the recharge area as the difference between spring elevation and maximum elevation of the area contributed by recharge. The relief was calculated for the recharge areas as well as for squares with size of 5 km² around the random points. Further, I performed GIS analysis to calculate the distances between the springs to the nearest fault. Due to the lack in available fault data I did this calculation for 198 springs and 441 random points. A map of the considered springs is shown in fig. 4.

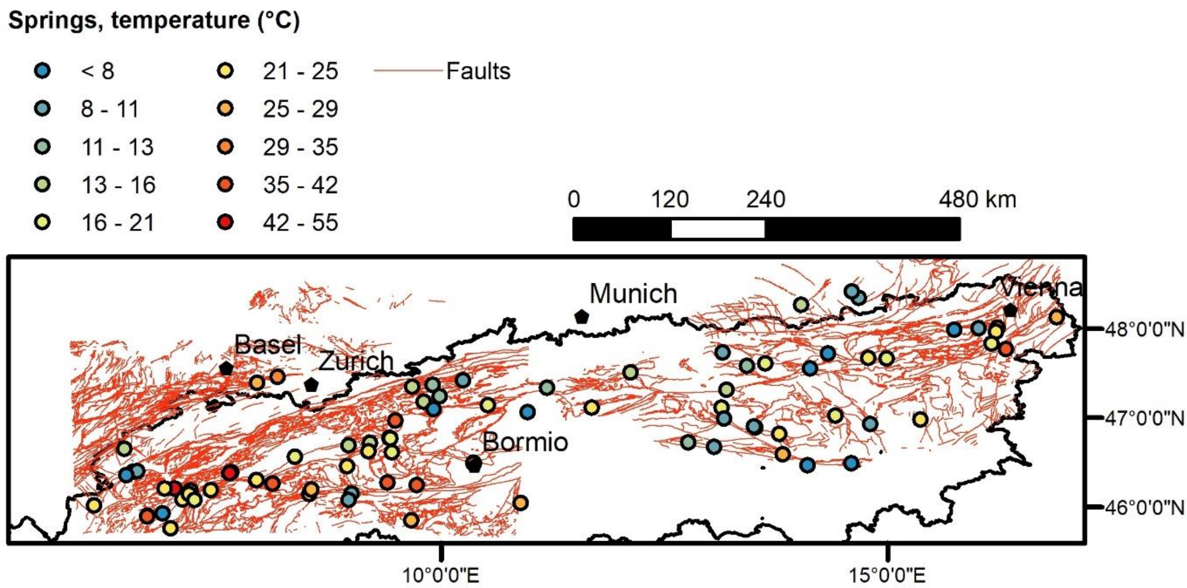

Figure 4: Fault data and the thermal springs used for the calculation of the distance between springs and faults. The colors of the dots represent the flow rate at the spring.

3.4 Background heat flow

To calculate the contribution of the thermal springs to the total heat flow in the Alps I estimated a background heat flow of 0.0665 W and an area of the Alps of 258 × 10^3 km² (ESDAC). The background heat flow is the average heat flow of the Alps, which I calculated using 434 data points from the global heat flow database by Hasterok (in prep.). The maximum value in this data is at 0.11 ± 0.010 W and the minimum at 0.041 ± 0.01 W. In addition, I constructed an interpolated heat flow map (fig. 5, 6 and 7) using inverse distance weighting with a 469 × 300 cells grid.

3.5 Thermal model of the Bormio thermal springs

To calculate the thermal history of the spring and the surrounding rock I used a 2D inversed numerical model code, Beo (Luijendijk, submitted). The model code solves the implicit form of the advective and conductive heat flow equation

$$\rho_b \, c_b \, \partial T / \partial t = \nabla K \, \nabla T - \rho_f \, c_f \, \vec{q} \, \nabla T \qquad (5)$$

With ρ_b (kg m^{-3}) as bulk density and ρ_f as the density of the corresponding fluid which in this case is water. $c_{b,f}$ is the specific heat capacity (J K^{-1} kg^{-1}) and $\frac{\partial T}{\partial t}$ (K year^{-1}) is the change of temperature T (K) over time t (s). K is thermal conductivity (W m^{-1} K^{-1}), T is temperature (K) and q is the fluid flow (m s^{-1}). To model the heat transfer the code uses Escript (Gross et al., 2007), a generic finite element code.

The left hand side of eq. 5 shows the change in temperature over time. The first part of the right hand side term is conductive heat flow and the second part of the term is advection by fluid flow. Temperatures and heat flow at the land surface are controlled by latent and sensible heat flow (W m^{-2}) (Bateni and Entekhabi, 2012). This relation is shown in equation 6, where ρ is density (kg m^{-3}), c is the specific heat of air (J kg^{-1} K^{-1}), r_a is the aerodynamic resistance to heat transfer (s m^{-1}), T_a is the air temperature at a reference height (°C) and T_s is the surface temperature (°C) (Louis et al., 2018; Luijendijk, submitted).

$$H = \rho c / r_a \, (T_a - T_s) \tag{6}$$

$$\mathrm{LE} = \rho L / r_a (q_s - q_a) \tag{7}$$

Equation 7 by Bateni and Entekhabi (2012) gives latent heat flow (W m^{-2}) as a function of density ρ (kg m^{-3}), specific latent heat of vaporization L (J kg^{-1}), the aerodynamic resistance r_a and the difference between saturated specific humidity at the surface temperature q_s (kg kg^{-1}) and the humidity of the air q_a (kg kg^{-1}). We can rewrite this to the conductive heat flow equation to get a value for the heat transfer coefficient K_s for sensible heat flow (W m^{-2}) (eq. 8) and the heat transfer coefficient for latent heat flow K_l (eq. 9).

$$K_s = \rho c / (r_a \Delta z) \tag{8}$$

$$K_l = (\rho L \Delta z / r_a) \times ((q_s - q_a)/(T_s - T_a)) \tag{9}$$

In eq. 8 and 9 Δz is the distance between the land surface and a reference height (m). According to Liu et al. (2007) Δz is set to 1.8 m where in their case measurements for T_a and H were performed. For simplification I assumed that advection occurs only in the fault damage zone and not in the host lithology. In the numerical model I fitted the properties of the fault and the aerodynamic resistance r_a. The geothermal gradient is used to calculate the reservoir temperature of the water which I assume to be in equilibrium with the surrounding rock. I modelled the discharge temperature of the spring and compared them to the measured temperatures. All the measured and modelled values for the best fitting simulation as well as the grid sizes for running a stable simulation are given in table 1. Whereas the flow rate at the springs is measured in m^3 s^{-1} the two dimensional model code uses fault flux in m^2 $year^{-1}$. I divided the sum of all ten measured flow rate values by the fault length perpendicular to the model domain. For fault length I used the maximum distance of thermal springs along the fault (700 m). I assumed a width of the damage zone of 50 m. The dip of the fault is set to 65 °, as interpreted from our own and previously published regional mapping (Froitzheim et al., 1994; Volpi et al., 2017).

Table 1: Fixed parameters for the Bormio thermal system

Parameter	Value	Unit	Reference
Width of model domain	2000	m	
Total depth of model domain	4000	m	
Air height	10	m	
Cell size	100	m	
Cell size air layer	5	m	
Cell size upper layer	50	m	
Cell size fault	5	m	
Cell size base	500	m	
Size of time step	2	years	
air temperature	5.4	° C	[2]
thermal conductivity dolomite/carbonate	1.33	W m^{-1} K^{-1}	[1]
thermal conductivity metamorphic basement	2.5	W m^{-1} K^{-1}	[1]
porosity dolomite/carbonate	0.025		[1]
porosity metamorphic basement	0.01		[1]

[1] Volpi et al. 2017, [2] this work

3.6 Model sensitivity analysis

The spring temperature depends for instance on heat capacity of the surrounding rock, depth of the fault, width of the damage zone and geothermal gradient. Whereas lithological parameters and fluid flow are known from field work or literature (Volpi et al., 2017), other parameters like fault depth remain unknown. To explore the influence of the value of each parameter to the change of the spring temperature and to the temperature at depth I performed a sensitivity analysis for six parameters: Air temperature (°C), fault flux (m^2 $year^{-1}$), fault depth (m), geothermal gradient (K m^{-1}), aerodynamic resistance (s m^{-1}) and width of the damage zone (m). For each part of the sensitivity analysis I changed only one of the six parameters. The others are set to a constant base value. The base values and the range of the tested parameter values are listed in table 2. Based on this sensitivity analysis I refined the parameters for the model described in sec. 3.5.

Table 2: Constant values for each sensitivity analysis and the simulated temperature resulting from base run.

Parameter	Base value	Range	Unit
Air temperature	5	3.5 – 8.5	°C
Fault flux	1200	500 – 1700	m^2 $year^{-1}$
Fault depth	1400	600 – 2000	m
Geothermal gradient	0.03	0.03 – 0.07	K m^{-1}
Aerodynamic resistance	100	25 – 200	s m^{-1}
Fault damage zone width	50	40 – 120	m
Temperature	24.15	na	°C

4. Results

4.1 Heat contribution

Figures 5 and 6 show an interpolated surface heat flow map based on the available data by Hasterok (in prep.). The maps show that in the southern part of the Western Alps and on the eastern boundary the heat flow (HF) is much higher than in the central Alps with values of up to 0.11 W. The contact between the eastern and western Alps (running from the area east of Zurich to SSW) occurs as a relatively cold area as compared to the rest of the Alps with values less than 0.05 W. In the western Alps the spring temperatures are higher than in the eastern Alps (fig. 6). However, the locations of the hotter springs are not connected to the spots with the highest HF. For the flow rate no correlation to background HF can be observed (fig. 5). I calculated HF for each spring and, based on the heat flow data, the contribution of the sum of all springs to the bulk heat budget as described in sec. 3.2 as the consequence of the difference between recharge and discharge temperature together with the corresponding fluid flow rate. HF of each spring is plotted to the interpolated heat flow map in fig. 7. There is no visible correlation between HF of the spring and the local background HF. In total, the alpine thermal springs have a heat flow of 1.5×10^8 – 2.2×10^8 W. Considering the distribution of heat flow of the springs (fig 5, 6 and 7) over an area of 2.58×10^5 km^2 and a calculated bulk heat flow of 0.066 W this makes a contribution of 0.9 – 1.3 % to the entire heat budget. An overview of values for the size of the area, number of springs etc. is given in table 3. Figure 8 shows histograms of the number of springs in the Alps plotted against discharge temperature, flow rate at the spring in logarithmic scale and heat flow of the springs. The contributed recharge area in the Alps amounts 2300 to 3300 km^2. The ranges are caused by the range in recharge temperature (sec. 3.2). The hottest of the 234 considered springs in the Alps is located in Acqui, Italy with a discharge temperature of 70.5 °C.

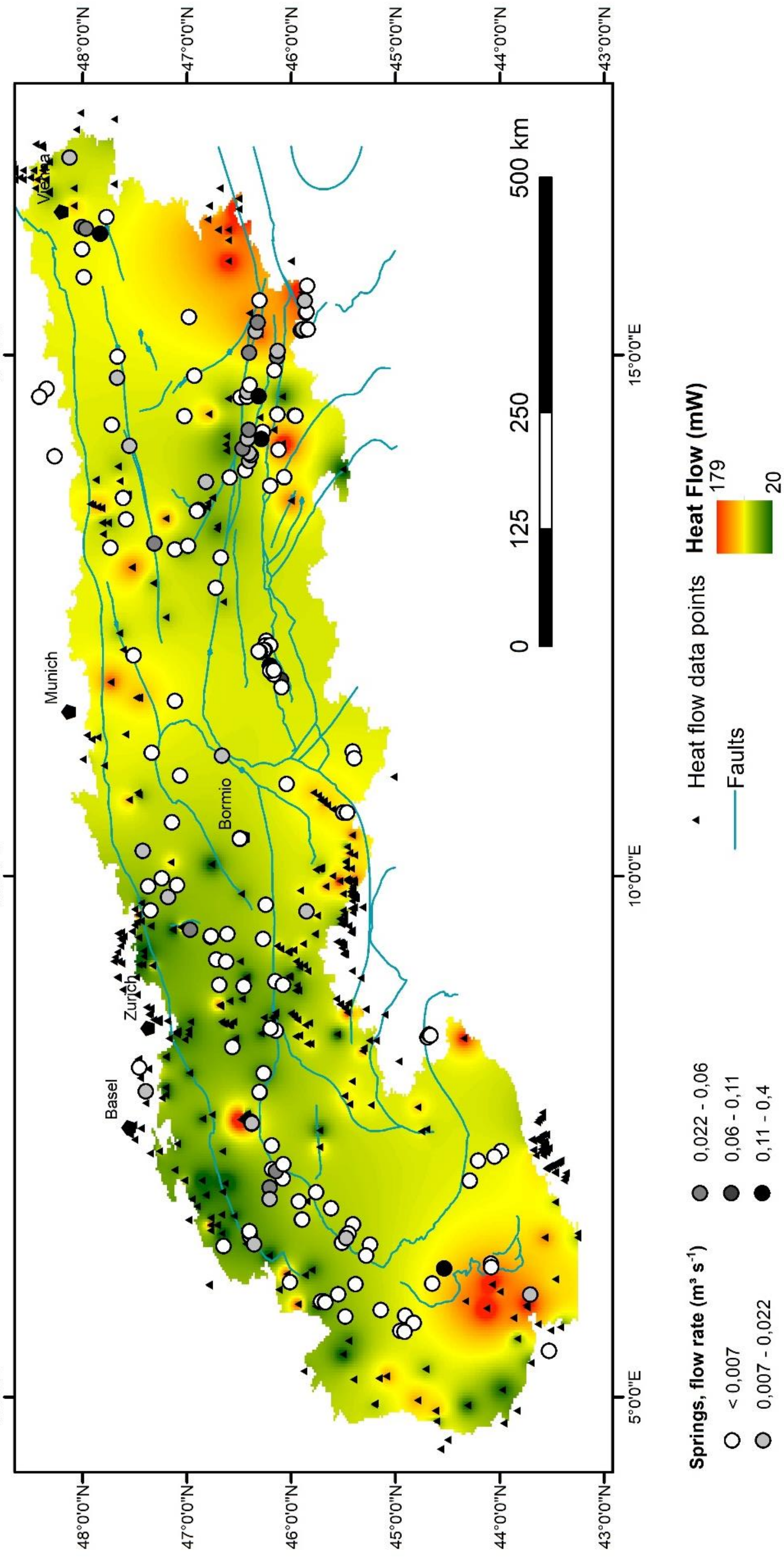

Figure 5: Interpolated heat flow map of the Alps showing the location of the 234 thermal springs and their flow rate ($m^3\ s^{-1}$). The triangles represent the 596 data points from Hasterok (in prep.) used for the interpolation.

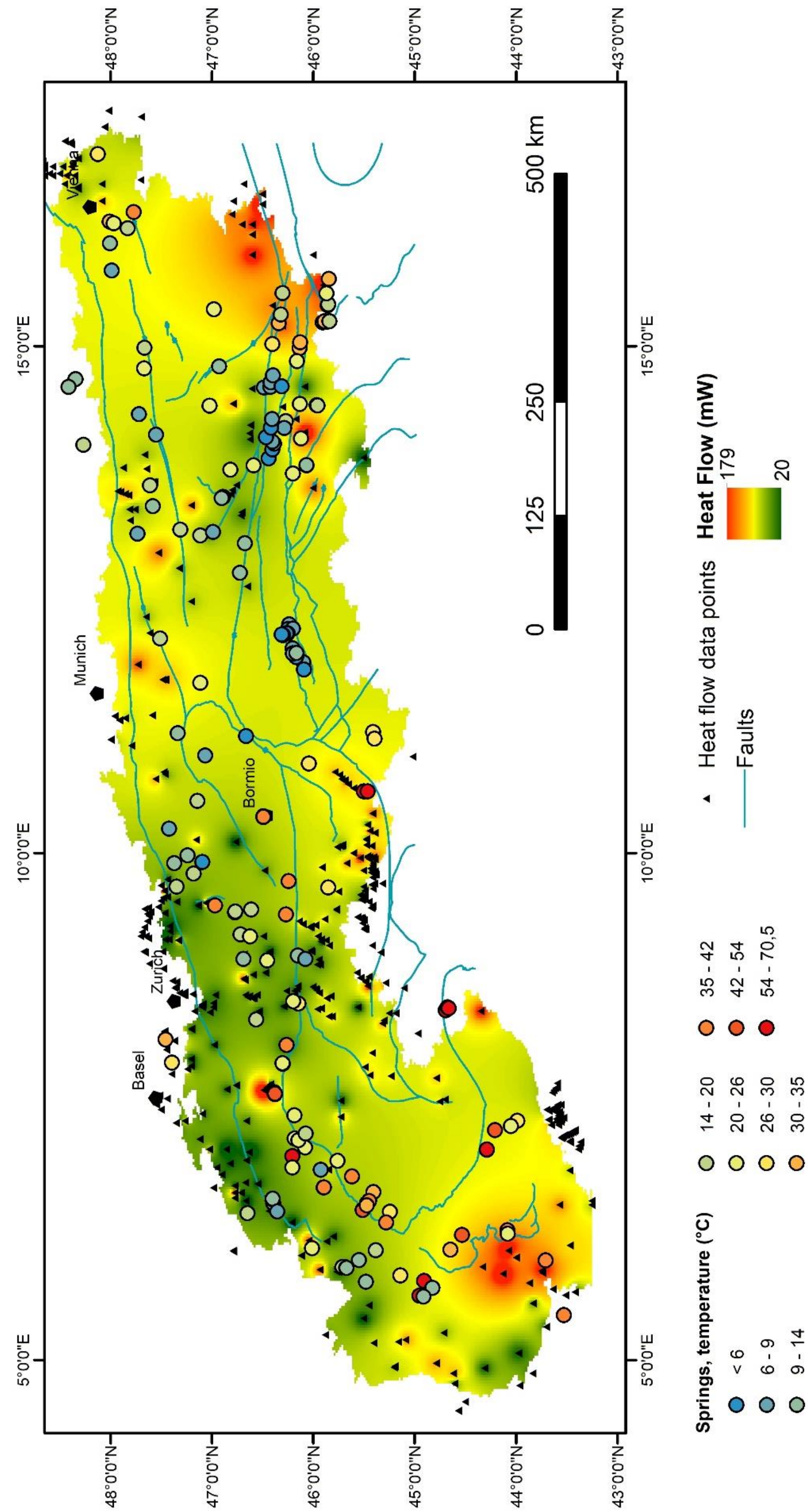

Figure 6: Interpolated heat flow map of the Alps showing the location of the 234 thermal springs and their temperatures (°C). The triangles are the 596 data points from Hasterok (in prep.) used for the interpolation.

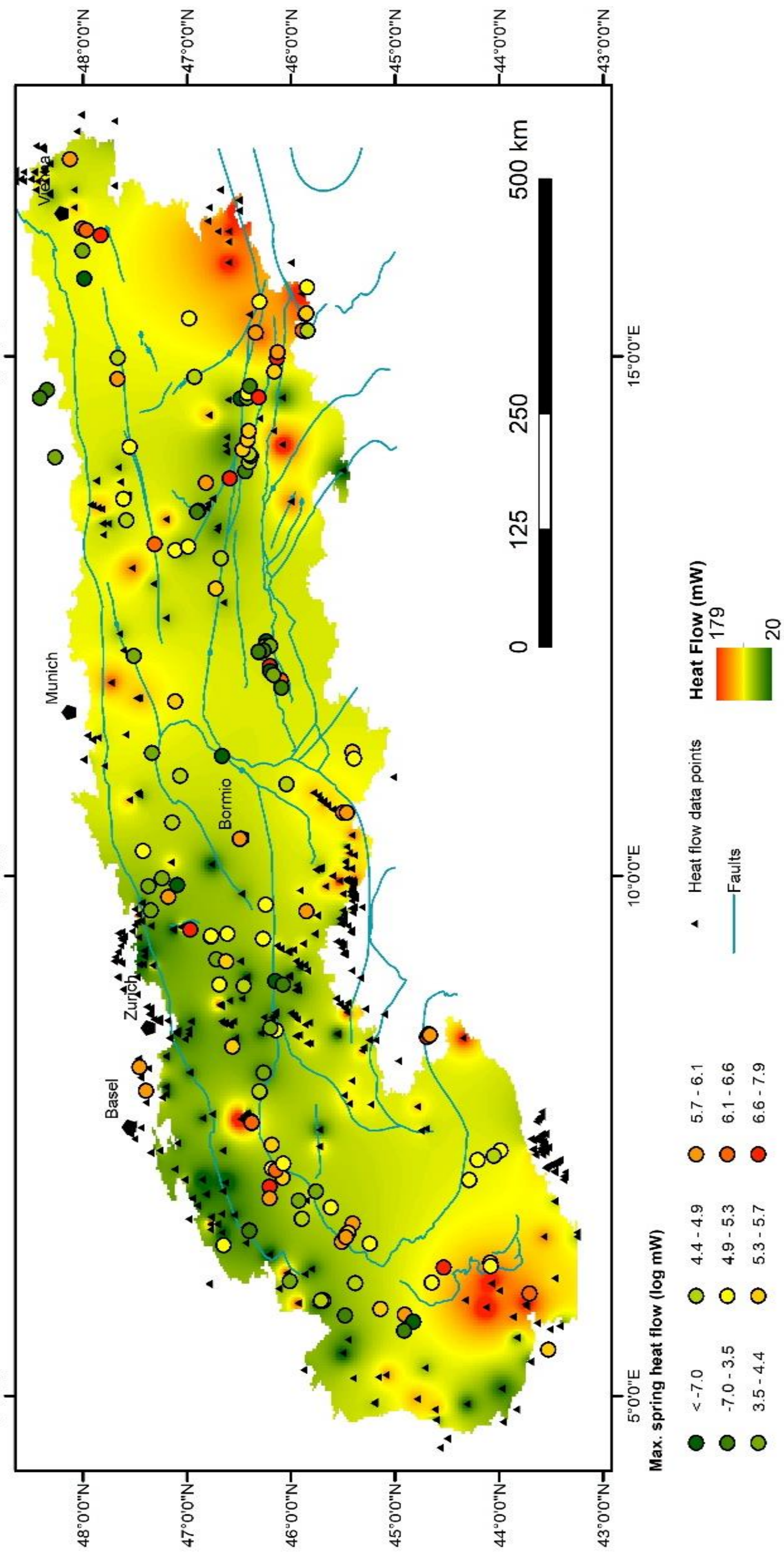

Figure 7: Interpolated heat flow map of the Alps showing the location of the 234 thermal springs and their heat flow (log mW) calculated as in sec. 3.2. The triangles are the 596 data points from Hasterok (in prep.) used for the interpolation.

Table 3: Values used for modelling the contribution of thermal springs to the total heat flow in the Alps and in the Basin and Range system in Nevada.

	Unit	Alps	Reference	Nevada	Reference
Total area	km^2	258 000	[2]	286 000	[3]
Contributing area	km^2	2 270 – 3 260	[1]	5 480	[1]
Number of springs		234	[1]	118	
Bulk heat flow	W	0.066	[1]	na	
Heat flow of the springs	W	$1.5 \times 10^8 - 2.2 \times 10^8$	[1]	4.2×10^8	
Contribution	%	0.9 – 1.3	[1]	1.9	[1]

References: [1] This work, [2] ESDAC, [3] Ferguson, G. and Grasby, S. E. (2011)

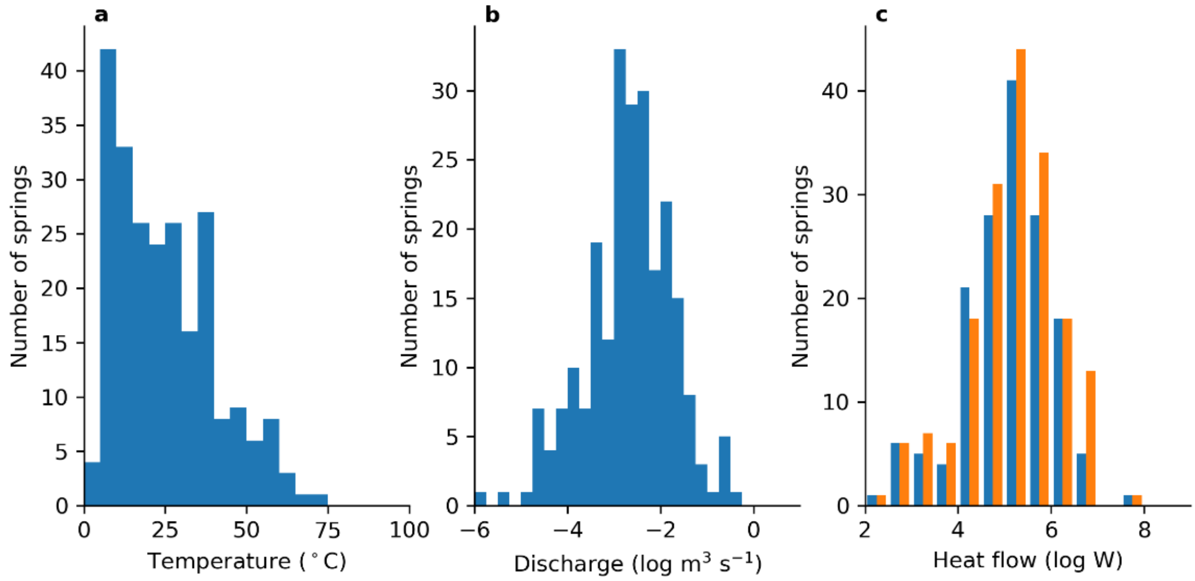

Figure 8: The histograms show the number of springs in the Alps plotted against a) discharge temperature (°C), b) flow rate ($m^3 s^{-1}$) in logarithmic scale and c) minimum (blue) and maximum (orange) heat flow (W) in logarithmic scale.

4.2 Statistics

For statistics I compared the spring properties from the database mentioned in sec. 3.1 to the average Alps. The histograms in fig. 9 show elevation, the relief of the recharge area, the lithology and the distance to the nearest fault of the springs (blue frames) and of the random points (grey bars). The springs tend to higher elevations and higher reliefs than the random points. While a maximum of 37 % of the squares around the points in the Alps has a shallow relief (less than 250 m), the relief of the recharge area varies more and does not show such a maximum. Only 11 % of the springs have a recharge area with a relief less than 250 m. The bars in fig. 9a show that the area with a certain elevation decreases continuously with the increase in elevation. However, the number of springs for elevations under 750 m.a.s.l. increases with the altitude. Above 750 m.a.s.l. the number decreases to 47 springs. In total 55 % of the springs and of the random points are elevated below 750 m. But 23 % random points against 9 % of the springs are located below 250 m elevation. Figure 9c shows the distribution of the springs in different lithologies. The most frequent lithology is carbonate rocks, followed by unconsolidated sediments and crystalline rocks. This distribution is relatively represented by the lithologies hosting springs. Thus, 41 % of the springs emerge in carbonates. Siliciclastic sediments are rare compared to other lithologies. However, 9% of all springs emerge in siliciclastic sediments, compared to < 2 % of random points. The histogram in figure 9d shows the distance of the springs and the random points to the nearest fault. 47 % of the springs are closer than 500 m to the nearest fault, compared to 25 % of random points. The distribution of random points is shifted to higher distances compared to the spring. Fault kinematics and the geological structure that is responsible for the spring (e. g. springs may be caused by karst systems) were not considered in this calculation. In figure 10 discharge temperature (°C) and flow rate ($m^3\ s^{-1}$) are plotted against surface lithology. Carbonates provide the highest flow rates, followed by mixed sediments and unconsolidated sediments. Due to a high number of springs with low flow rates, this is not generally valid but for single springs. For the discharge temperatures there is no correlation. Also, neither flow rate nor discharge temperature show a correlation to the distance to the next fault (fig. 11 and 12).

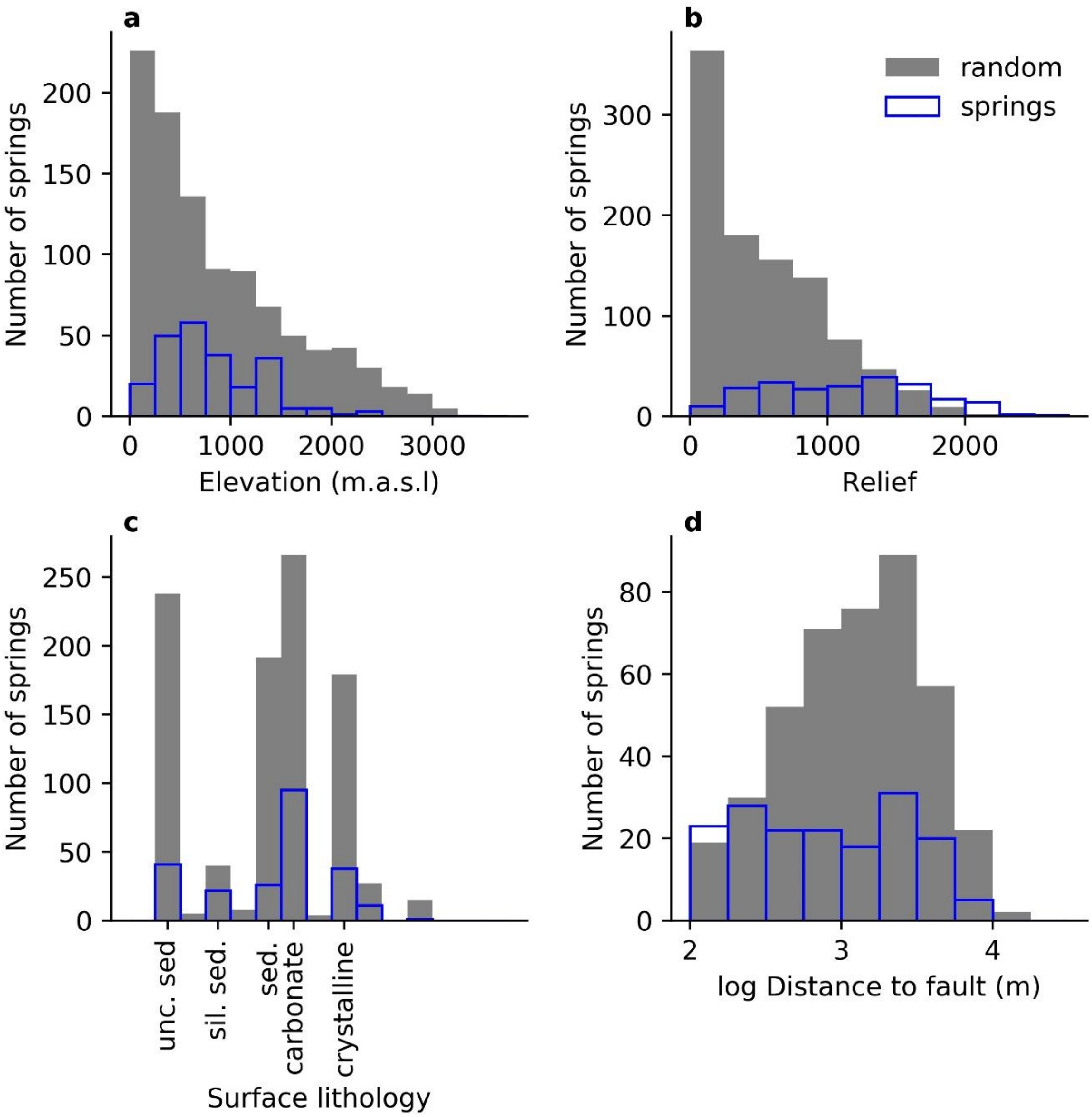

Figure 9: These histograms show in the blue frames the number of springs plotted against a) elevation (m.a.s.l.), b) relief of the area contributes recharge (m), c) surface lithology where the springs emerge and d) the distance to the nearest fault (m) in logarithmic scale. The grey bars are the number of random points distributed over the Alps. The relief of the random points is calculated for a constant size of 5 km². In c): unc. sed = unconsolidated sediments, sil. sed. = siliciclastic sediments, sed. = sediments.

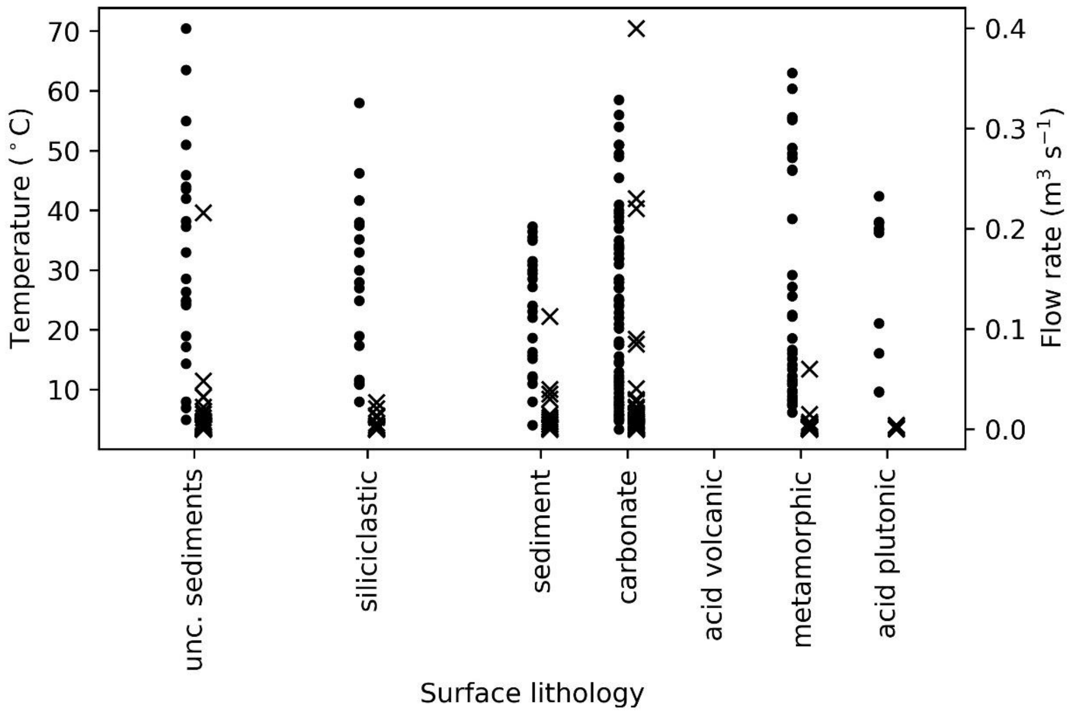

Figure 10: Dots represent the discharge temperature (°C) and the x represents the flow rate (m³ s^{-1}) at the springs on the vertical axis. The horizontal axis shows the corresponding surface lithology.

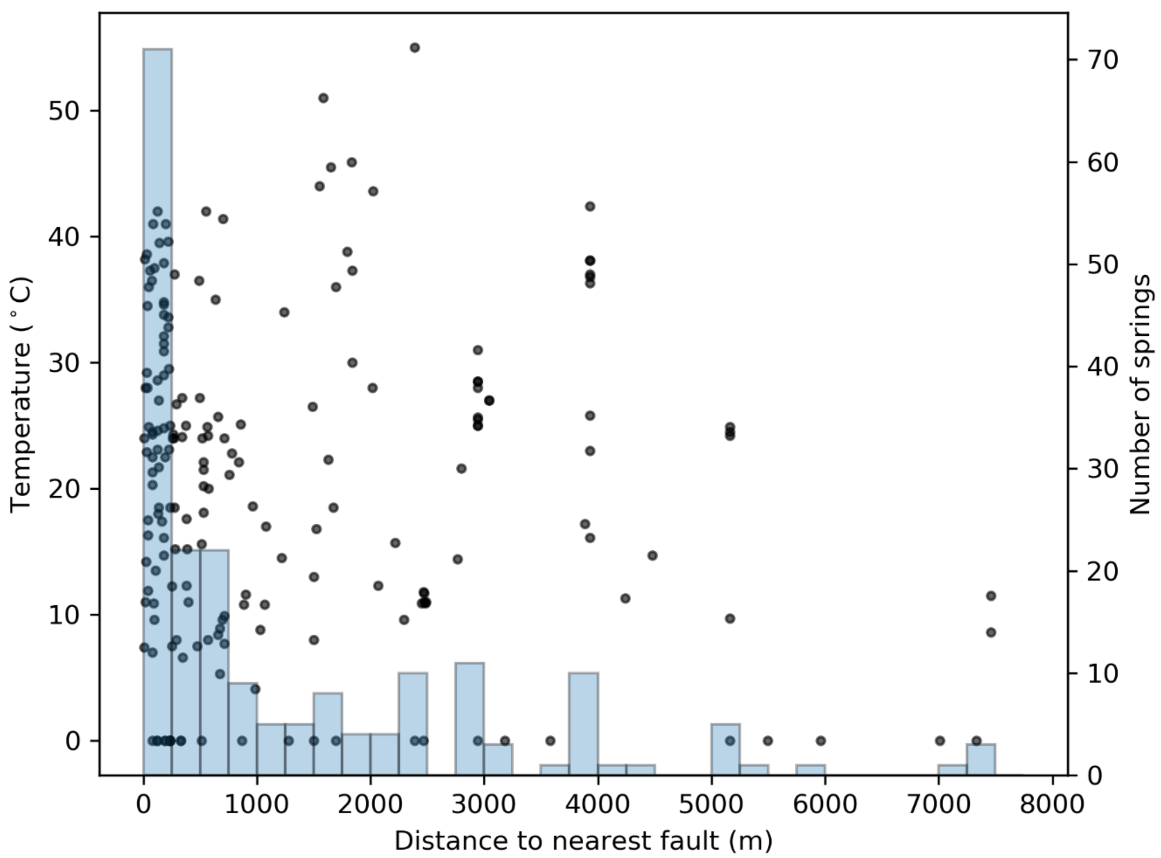

Figure 11: The distance to nearest fault (m) on x-axis is plotted against the discharge temperature (°C) and against the number of springs.

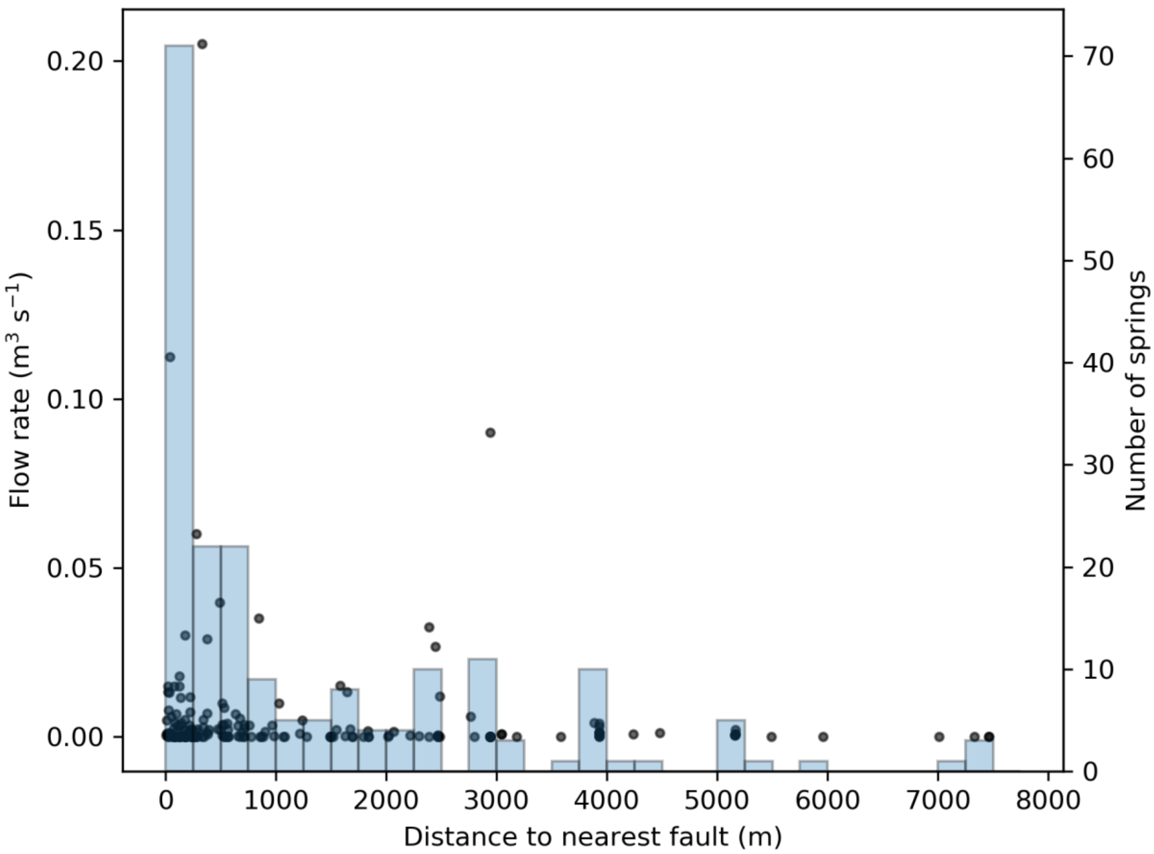

Figure 12: The distance to nearest fault (m) on x-axis is plotted against the flow rates ($m^3\ s^{-1}$) and against the number of springs.

4.3 Numerical modelling of the Bormio spring system

The ten springs in the Bormio hydrothermal system have an average discharge temperature of 38 °C. The mean fault flux is 170 $m^2\ year^{-1}$. In sum the discharge of all spring in the Bormio hydrothermal system is 1700 $m^2\ year^{-1}$. Figure 13 shows the temperature development simulated for the average fault flux (blue line) and for the overall system (orange line). All other parameters are the same for both simulations and listed in table 4. In both cases the maximum surface temperature reaches the steady-state temperature (see sec. 4.3) after 300 years. The lower part of figure 14 contains schematic cross sectional views of the fault which causes the upward fluid flow for the beginning of the model run, after 150 years and after 500 years. The colours represent the temperature in subsurface. The upper subplots show the surface temperature which correlates at the spring with the discharge temperature. Figure 15 shows the corresponding results for the simulation with the average fault flux of 170 $m^2\ year^{-1}$. The figures show that the area in direct contact to the fault receives the highest temperature increase since the beginning of the model run (fig. 14a) and 15a) for surface temperature and 14d) and 15d) for subsurface temperature). For a fault flux of 1700 m² year $^{-1}$ the subsurface is affected to a distance of 430 m at a depth of 500 m around the fault and a distance of 390 m at a depth of 1000 m. This distance is decreasing towards land surface. The simulated reservoir temperature at the depth of 2200 m is 80 °C. At the fault depth of 1000 m the modelled temperature is 77 °C. At land surface the affected area has a radius of 50 m. At the spring the temperature reaches 38 °C. For the fault flux of 170 m² year $^{-1}$ the affected area at 1000 m depth has a distance of 195 m from the fault. At depth of 500 m the area has a radius of 180 m. The maximum temperature at the depth of 1000 m is 57 °C. The simulated reservoir temperature for this fault flux is 79 °C. There is no effect on the land surface temperature for this low fault flux. The modelled discharge temperature after 500 years is 8 °C. Due to the steady-state temperature shown in fig. 13 there is no significant increase to expect for the further development. Both calculations show that the affected area is increasing with time. The longer the springs system is active, the larger is the heated area. All mentioned simulated values are listed in table 4. Table 5 contains the parameter values which I used for the best fitting simulation.

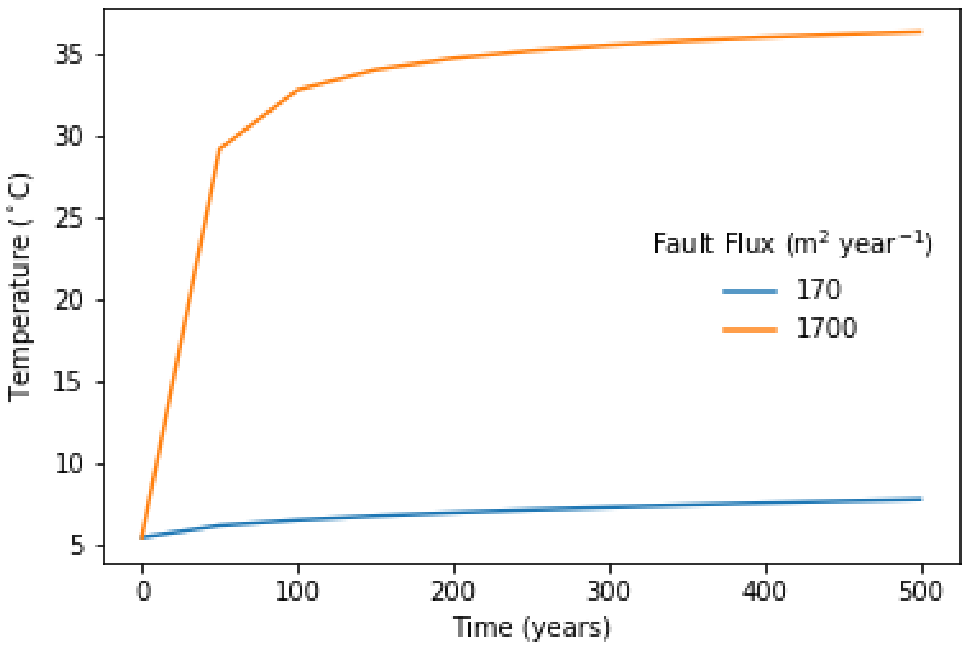

Figure 13: Discharge temperature (°C) on the vertical axis is plotted against time (years) on the horizontal axis. The two lines represent the temperature development (°C) for two different fault fluxes over time. 170² year $^{-1}$ (blue line) is the average fault flux at the faults for the Bormio thermal spring system. 1700 m² year $^{-1}$ (orange line) is the sum of all ten thermal springs. All other parameters are the same.

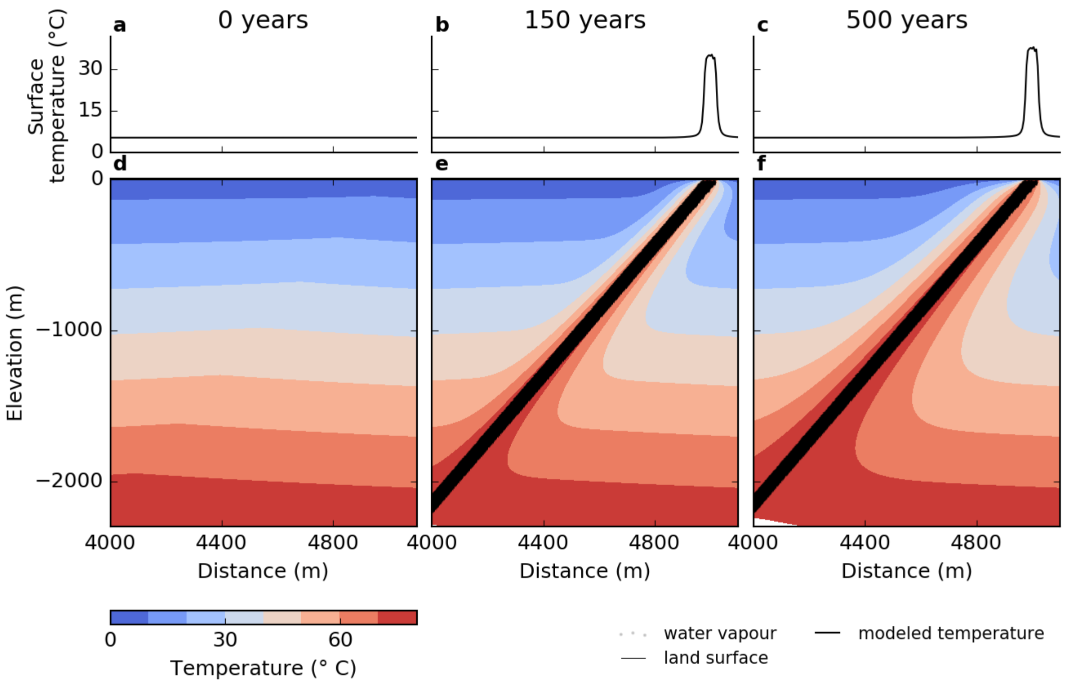

Figure 14: a) to c) show the surface temperature (°C) in a) the beginning of the model run, b) after 150 years and c) after 500 years. d) to f) show the subsurface temperature (°C) for the same time steps. The black bar represents the fault. The fluid flux is 1700 m² year^{-1} for this model run.

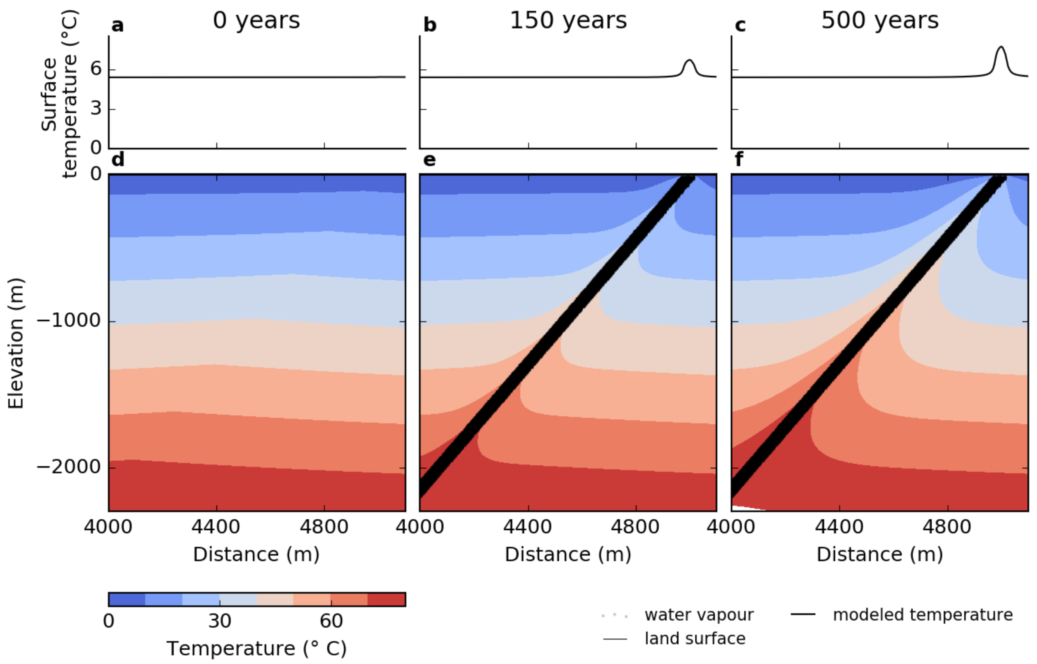

Figure 15: a) to c) show the surface temperature (°C) in a) the beginning of the model run, b) after 150 years and c) after 500 years. d) to f) show the subsurface temperature (°C) for the same time steps. The black bar represents the fault. The fault flux is 170 m² year^{-1} for this model run.

Table 4: Fitted model parameters

Parameter	Values	Unit
Measured flow rate (summed)	0.04	$m^3\ s^{-1}$
Fault flux	0.055	$m^2\ s^{-1}$
Input fault flux	1700	$m^2\ year^{-1}$
Fault depth	-2200	m
Fault angle	65	°
Width of the damage zone	50	m
Aerodynamic resistance	120	$s\ m^{-1}$
Geothermal gradient	0.03	$K\ m^{-1}$
Basal heat flow	0.066	W

Table 5: Modelled temperatures for two values of fault flux (1700 m² $year^{-1}$ and 170 m² $year^{-1}$) after 500 years of model run. Listed are water temperatures for land surface and the depth of 1000 m. Further the affected distance from the fault is listed for land surface and the depth of 500 m and 1000 m.

	1700 $m^2\ year^{-1}$	170 $m^2\ year^{-1}$	Unit
Spring temperature	38	8	°C
Temperature at 1000 m depth	77	57	°C
Temperature at 2200 m depth	80	79	°C
Affected distance at land surface	50	0	m
Affected distance at 500 m depth	430	180	m
Affected distance at 1000 m depth	390	195	m

4.4 Sensitivity analysis

I performed a sensitivity analysis for the parameters aerodynamic resistance (s m^{-1}), air temperature (°C), fault flux (m² $year^{-1}$), depth of the fault (m), width of the damage zone (m) and geothermal gradient (°C m^{-1}). The results are shown in fig. 16 and 17. The vertical axis in fig. 16 shows the discharge temperature (°C) and the horizontal axis shows the ratio between the used parameter value to a constant base value. The discharge temperature shows the strongest sensitivity to the change in the geothermal gradient, followed by the fault parameters depth and width of the damage zone and the fault flux. The width of the damage zone is inversely correlated with discharge temperature. An increase of the width of the damage zone causes a decrease in temperature. The sensitivity to aerodynamic resistance is nonlinear. Until the base value of 100 s m^{-1} (ratio = 1) the curve is close to the curves of fault flux and fault depth. For ratios over 1 the increase in the caused discharge temperature gets less with the increase in aerodynamic resistance. The change in discharge temperature of the spring shows the lowest sensitivity to the air temperature. Here an increase in the parameter value shows an increase in the temperature as well.

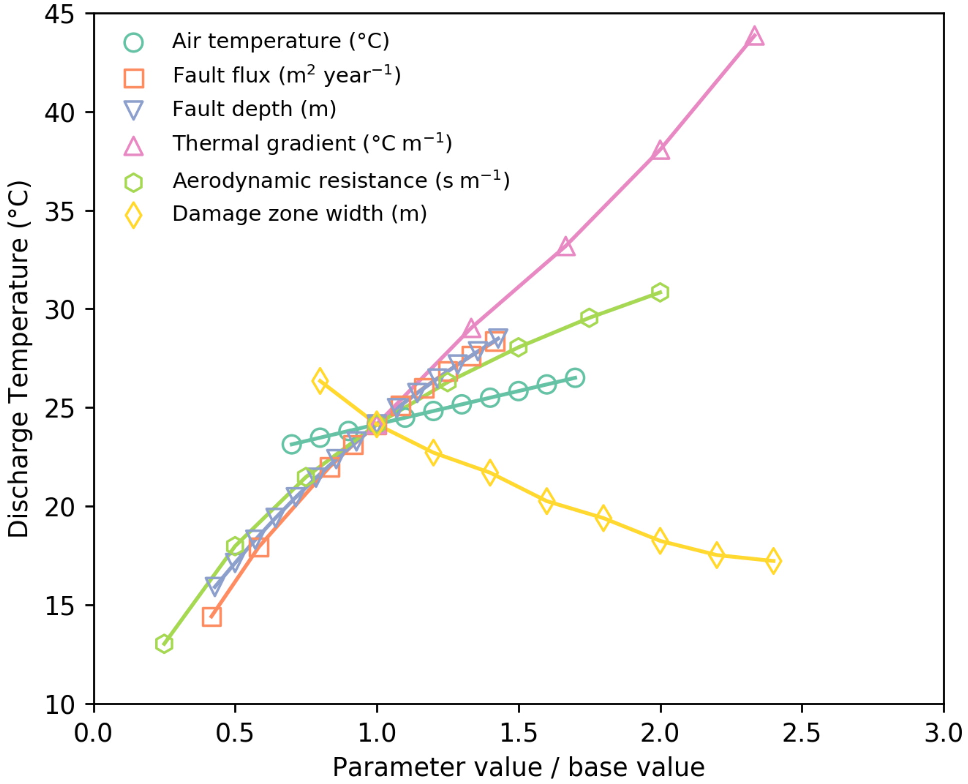

Figure 16: Sensitivity analysis of the discharge temperature performed for the following six parameters: Air temperature, fault flux, depth of the fault, geothermal gradient, aerodynamic resistance and width of the damage zone. Base values are 5 °C air temperature, fault flux of 1200 m² $year^{-1}$, fault depth of 1400 m, a thermal gradient of 0.03 K m^{-1}, the aerodynamic resistance is set to 100 s m^{-1} and the damage zone width to 50 m. The horizontal axis shows the ratio of the parameter value to its base value.

In fig. 17 the development of the discharge temperature is plotted over time forfive sensitive parameters (aerodynamic resistance, fault flux, width of the damage zone, fault angle and fault depth). For all of these parameters, temperature shows the development of a steady-state after a duration of 100 to 350 years. At steady-state the increase in temperature is lower than 0.2 °C and is continuously decreasing. The steady-state develops without a significant dependenceon the parameter values. The parameter values only change the spring temperature, not the response time of the springs.

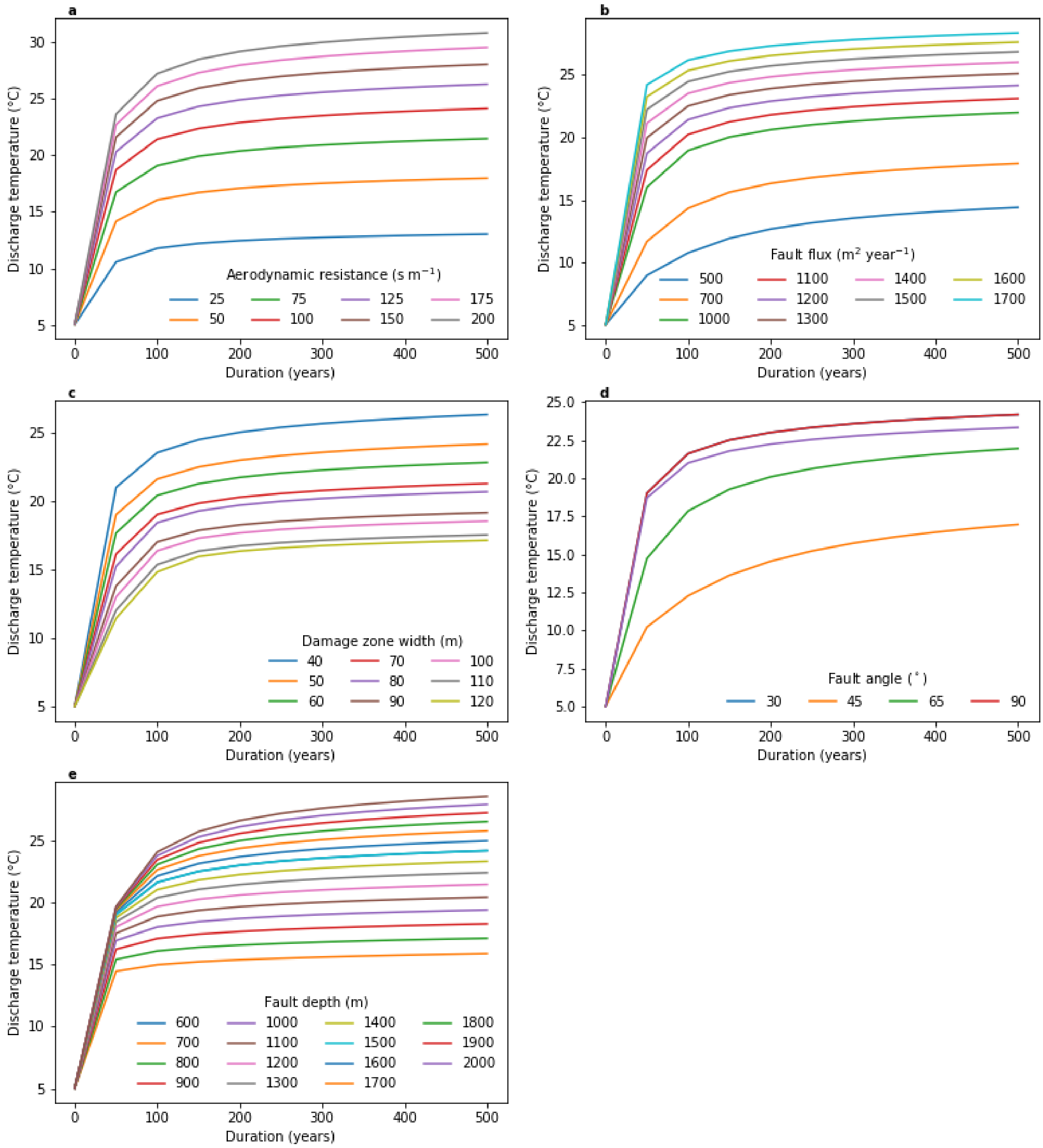

Figure 17: Development of the discharge temperature (vertical axis) (°C) over time (years) for the sensitivity analysis of a) the aerodynamic resistance (s m^{-1}), b) the fault flux (m^2 year^{-1}), c) the width of the damage zone (m), d) the dip angle of the fault (°) and e) the fault depth (m). Each line shows the temperature development for one value of the sensitive parameter.

5. Discussion

5.1 Heat contribution

I calculated a contribution of 0.9 – 1.3 % of 234 spring to the entire heat budget in the Alps. According to Luijendijk (unpublished) the contribution of the thermal springs in the Basin and Range system in Nevada accounting 1.9 % to the entire heat budget. This is slightly higher than the contribution of the springs in the Alps. As described in sec. 4.1 and listed in table 3, the heat flow of the springs in Nevada is with 4.2×10^8 W twice as high as the heat flow of the springs in the Alps. However, the area of the Basin and Range Province has an anomalously thin lithosphere. The temperatures and therefore, the heat flow of the springs is much higher than in the Alps. 20 of all the springs in Nevada have temperatures of more than 75 °C (fig. 18), whereas in the Alps 70.5 °C is the maximum measured discharge temperature. The expected difference in the contribution of these two regions was much higher. With a total number of 234 thermal springs, the Alps host almost double the amount of thermal springs than in the Basin and Range with a reported amount of 118 springs in Nevada. Thus, the large abundance of thermal springs in the Alps results in a similar contribution to the entire heat budget as in Nevada.

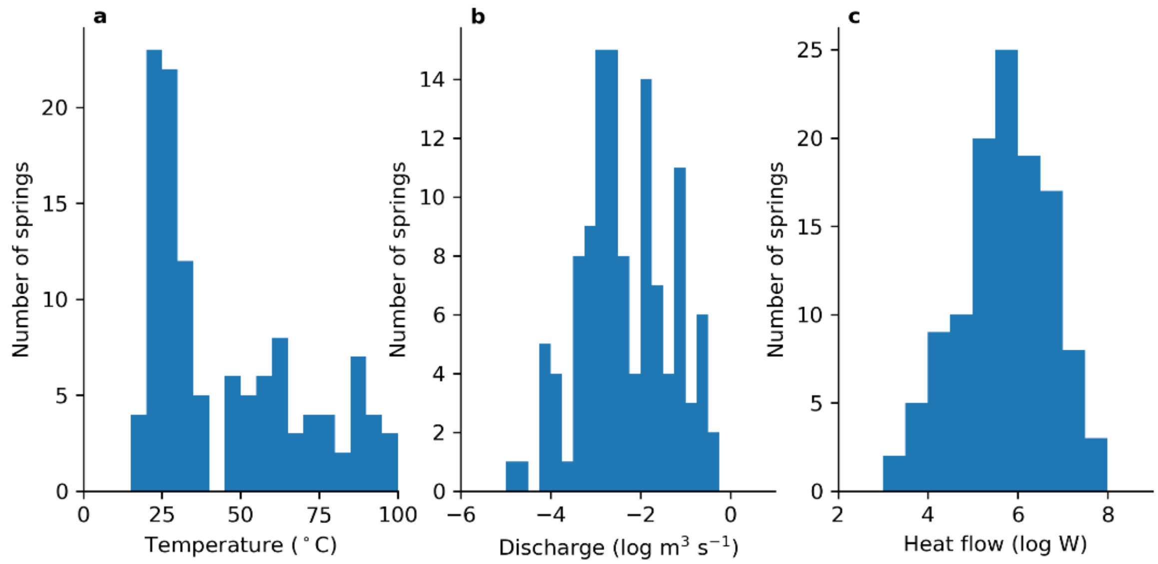

Figure 18: These histograms show the number of springs in Nevada plotted against a) discharge temperature (°C), b) spring discharge (m^3 s^{-1}) in logarithmic scale and c) heat flow (W) in logarithmic scale.

5.2 Distribution of springs

Due to the high amount of carbonates in the Alps an expected number of 41 % of the springs emerge in carbonate rocks. More unexpected is the high relative value of 9 % of springs which emerge in siliciclastic sediments. More than half of the springs have a distance less than 1 km to the nearest fault (fig. 9) and 47 % have a distance less than 500 m to the nearest fault. However, I was not able to determine a relation to the geological structure responsible for the occurrence of the springs. The correlation between the character of the spring and fault systems would be worth for further investigation.

5.3 Temperature development

The simulations in sec. 3.4 and 3.5 show the development of a steady-state temperature for the Bormio thermal spring system after 100 – 350 years. However, Volpi et al. (2017) proposed a duration of 13000 years to reach the mean temperatures of 38 °C. Due to a three dimensional hydrothermal system solved with a two dimensional model code I used the summed fault flux of 1700 m^2 $year^{-1}$ of all springs in the Bormio hydrothermal system to reach this mean temperature. For simplification I set this fault flux as constant for the entire duration. According to Volpi et al. (2017) the increasing melting of permafrost causes a continuous increase in recharge over time. For my simulation I had to consider that in the beginning of the simulation the fault flux might be less than 1700 m^2 $year^{-1}$. Due to glaciation circulating water is assumed to be less than in present time. However, according to Person et al. (2007) infiltration of meltwater must not be neglected due to its contribution to the circulation of ground water. Therefore, I assess my simplification as reasonable. Further, the age of the spring system cannot be determined by the simulation presented in this work.

6. Conclusion

I used a new thermal spring database of the Alps and the global recharge database by de Graaf (2017) to calculate the contribution of thermal springs in the Alps to the overall heat budget. The resulting 0.9 – 1.3 % of contribution is the first calculation which was done for an entire orogen. I calculated the minimum distance between springs and faults. The calculation and maps show that springs occur preferably in the vicinity of faults. For a case study I calculated the thermal history of the Bormio hydrothermal system. The simulation shows the development of a steady-state temperature after 100 – 350 years. The measured mean temperature in the Bormio thermal system is 38 °C. This temperature can only be modelled if the fault depth is assumed to be 2200 m below surface. At depth the simulated maximum temperature is 80 °C. To reach the measured and simulated temperatures I propose two options for the pathway of upward fluid flow. The first is that the base of the Zebrù Thrust lays 800 m deeper than previously assumed. Second, if the S dipping Gallo Fault continues further to depth and cross cuts the Zebrù Thrust fluid may flow along this fault.

7. Acknowledgement

First of all, I want to thank my first supervisor Dr. Elco Luijendijk. You have been very patient with all my sometimes ridiculous questions, weird thoughts and annoying programming and software problems. I was really lucky to have such a good mentor. I feel a little bit nerdy now.

Thanks to my second supervisor Dr. Christoph von Hagke for all the constructive comments and discussions which really provided a lot of good ideas and helped me to improve my thesis. You gave me a lot confidence and showed me future perspectives.

Thanks to Elco, Christoph, Martin, Biggi, Sarah and Theis for reading, correcting, commenting, criticizing… my thesis. Repetitions of names at this point are intentions! You spent really a lot of time with this.

Thanks again to Elco, Christoph and Theis for the amazing time in the Alps. Without fieldwork and awesome views, geology makes only half as fun as it does.

Thank you Sarah for the coffee machine and for all the time and help you always offered to me.

I want to thank the entire department of structural geology for the awesome atmosphere.

I have to thank my dear Martin. Du hast mir jederzeit, in allen denkbaren Situationen bis zum letzten Tag den Rücken freigehalten. Ohne deine Unterstützung hätte ich diese Arbeit nicht schreiben können.

Lea, Karl und Minna! Die niedlichsten, zotteligsten und tollsten Kinder, die man sich wünschen kann. Ihr habt eine Menge einstecken müssen. Diese Etappe haben wir nun geschafft! Ich danke euch für eure Geduld und hoffe, ihr werdet mir irgendwann nachsehen, dass ich so wenig Zeit für euch hatte.

Danke Susann für die Pausen mit Kaffee, im Roxx und auch mit Lifestyle-Getränk. Du hast mich an dem schwierigsten Punkt der letzten Monate wieder hochgezogen. Ganz nebenbei hast du mir auch noch ein paar nennenswerte Credits besorgt, die womöglich in Vergessenheit geraten wären.

8. References

Arcoraci, L., Battelli, P., Castellano, C., Marchetti, A., Mele, F., Nardi, A., Pirro, M. and Rossi, A.: Bollettino Sismico Italiano 2009, , 99(10-Apr-2012) [online] Available from: http://hdl.handle.net/2122/7931, 2012.

Artemieva, I. M., Thybo, H. and Kaban, M. K.: Deep Europe today: geophysical synthesis of the upper mantle structure and lithospheric processes over 3.5 Ga, Geol. Soc. London, Mem., 32(1), 11–41, doi:10.1144/GSL.MEM.2006.032.01.02, 2006.

Bateni, S. M. and Entekhabi, D.: Relative efficiency of land surface energy balance components, Water Resour. Res., 48(4), 1–8, doi:10.1029/2011WR011357, 2012.

Calais, E., Nocquet, J.-M., Jouanne, F. and Tardy, M.: Current strain regime in the Western Alps from continuous GPS measurements , 1996-2001, Geology, 30(7), 651–654, doi:10.1130/0091-7613, 2002.

Conti, P., Manatschal, G. and Pfister, M.: Synrift sedimentation, Jurassic and Alpine tectonics in the central Ortler nappe (Eastern Alps, Italy), 1994.

CREGE: Laboratoire de Géothermie, [online] Available from: https://crege.ch, n.d.

D'Agostino, N., Cheloni, D., Mantenuto, S., Selvaggi, G., Michelini, A. and Zuliani, D.: Strain accumulation in the southern Alps (NE Italy) and deformation, , 32(14-Oct-2005), doi:10.1029/2005GL024266, 2005.

Danielson, J. and Gesch, D.: Global Multi-resolution Terrain Elevation Data 2010(GMTED2010), U.S. Geol. Surv., 2010, 26, doi:citeulike-article-id:13365221, 2011.

DeMets C., R.G., G., D.F., A. and S., S.: Current plate motions, Geophys. J. Int., 101(2), 425–478, 1990.

Derry, L. A., Evans, M. J., Darling, R. and France-Lanord, C.: Hydrothermal heat flow near the Main Central Thrust, central Nepal Himalaya, Earth Planet. Sci. Lett., 286(1–2), 101–109, doi:10.1016/j.epsl.2009.06.036, 2009.

DWD: Deutscher Wetterdienst, [online] Available from: https://www.dwd.de/, n.d.

ESDAC: European Soil Data Centre, Alpine region boundary, [online] Available from: https://esdac.jrc.ec.europa.eu/projects/Alpsis/alpine_region_gis_data.html, n.d.

Ferguson, G. and Grasby, S. E.: Thermal springs and heat flow in North America, Geofluids, 11(3), 294–301, doi:10.1111/j.1468-8123.2011.00339.x, 2011.

Froitzheim, N., Schmid, S. M. and Conti, P.: Repeated change from crustal shortening to orogen-parallel extension in the Austroalpine units of Graubünden Graubünden Repeated change from crustal shortening to orogen- parallel extension in the Austroalpine units of, Eclogae Geol. Helv., 87(May 2014), 559–612, doi:http://dx.doi.org/10.5169/seals-167471, 1994.

Froitzheim, N., Conti, P. and Van Daalen, M.: Late cretaceous, synorogenic, low-angle normal faulting along the Schlinig fault (Switzerland, Italy, Austria) and its significance for the tectonics of the Eastern Alps, Tectonophysics, 280(3–4), 267–293, doi:10.1016/S0040-1951(97)00037-1, 1997.

Froitzheim, N., Plasienka, D. and Schuster, R.: Alpine tectonics of the Alps and Western Carpathians, in The Geology of Central Europe, Volume 2: Mesozoic and Cenozoic, edited by T. McCann, pp. 1141–1232, The Geological Society, London., 2008.

de Graaf, I. E. M., van Beek, R. L. P. H., Gleeson, T., Moosdorf, N., Schmitz, O., Sutanudjaja, E. H. and Bierkens, M. F. P.: A global-scale two-layer transient groundwater model: Development and application to groundwater depletion, Adv. Water Resour., 102, 53–67, doi:10.1016/j.advwatres.2017.01.011, 2017.

Grasby, S. and Hutcheon, I.: Controls on the distribution of the thermal springs in the southern Canadian Cordillera, Can. J. Earth Sci., 38(3), 427–440, doi:https://doi.org/10.1139/e00-091, 2001.

Gross, L., Bourgouin, L., Hale, A. J. and Mühlhaus, H.-B.: Interface modeling in incompressible media using level sets in Escript, Phys. Earth Planet. Inter., 163(1–4), 23–34, doi:https://doi.org/10.1016/j.pepi.2007.04.004, 2007.

Hartmann, J. and Moosdorf, N.: The new global lithological map database GLiM: A representation of rock properties at the Earth surface, Geochemistry, Geophys. Geosystems, 13(12), 1–37, doi:10.1029/2012GC004370, 2012.

Hasterok, D.: An analysis of the revised global heat flow database. [online] Available from: http://www.heatflow.org/, n.d.

Hormes, A., Ivy-Ochs, S., Kubik, P. W., Ferreli, L. and Michetti, A. M.: 10Be exposure ages of a rock avalanche and late glacial moraine in alta Valtellina, Italian Alps, Quartenary Int., 190(1), 136–145, doi:https://doi.org/10.1016/j.quaint.2007.06.036, 2008.

Husen, S., Bachmann, C. and Giardini, D.: Locally triggered seismicity in the central Swiss Alps following the large rainfall event of August 2005, Geophys. J. Int., 171(3), 1126–1134, doi:10.1111/j.1365-246X.2007.03561.x, 2007.

Ingebritsen, S. E., Sherrod, D. R. and Mariner, R. H.: Rates and patterns of groundwater flow in the Cascade Range Volcanic Arc, and the effect on subsurface temperatures, J. Geophys. Res. Solid Earth, 97(B4), 4–599, doi:https://doi.org/10.1029/91JB03064, 1992.

Kanduč, T., Mori, N., Kocman, D., Stibilj, V. and Grassa, F.: Hydrogeochemistry of Alpine springs from North Slovenia: Insights from stable isotopes, Chem. Geol., 300–301, 40–54, doi:10.1016/j.chemgeo.2012.01.012, 2012.

LGRB: Kartenviewer, Landesamt für Geologie, Rohstoffe und Bergbau, [online] Available from: http://maps.lgrb-bw.de/, n.d.

Liu, S., Lu, L., Mao, D., Jia, L. and Centre, R.: Evaluating parameterizations of aerodynamic resistance to heat transfer using eld measurements, Earth, (1), 769–783, 2007.

Louis, S., Luijendijk, E., Dunkl, I. and Person, M.: Episodic fluid flow in an active fault, , (November), doi:10.31223/osf.io/cjvxk, 2018.

Luijendijk, E.: Beo v1 . 0 : Numerical model of heat flow and low-temperature thermochronology in hydrothermal systems ., , 1–17, doi:10.31223/osf.io/e4gsp, 2018.

McInnes, B. I. A., Evans, N. J., Fu, F. Q. and Garwin, S.: Application of Thermochronology to Hydrothermal Ore Deposits, Rev. Mineral. Geochemistry, 58(1), 467–498, doi:https://doi.org/10.2138/rmg.2005.58.18, 2005.

Person, M., McIntosh, J., Bense, V. and Remenda, V. H.: Pleistocene hydrology of North America: The role of ice sheets in reorganizing groundwater flow systems, Rev. Geophys., 45(3), 1–28, doi:10.1029/2006RG000206, 2007.

Reiners, P. W. and Brandon, M. T.: Using Thermochronology to Understand Orogenic Erosion, Annu. Rev. Earth Planet. Sci., 34(3), 419–466, doi:doi: 10.1146/ annurev.earth.34.031405.125202, 2006.

Rolland, C.: Spatial and seasonal variations of air temperature lapse rates in alpine regions, J. Clim., 16(7), 1032–1046, doi:10.1175/1520-0442(2003)016<1032:SASVOA>2.0.CO;2, 2003.

Schlatter, A., Schneider, D., Geiger, A. and Kahle, H. G.: Recent vertical movements from precise levelling in the vicinity of the city of Basel, Switzerland, Int. J. Earth Sci., 94(4), 507–514, doi:10.1007/s00531-004-0449-9, 2005.

Ustaszewski, M. and Pfiffner, O. a.: Neotectonic faulting, uplift and seismicity in the central and western Swiss Alps, Geol. Soc. London, Spec. Publ., 298(1), 231–249, doi:10.1144/SP298.12, 2008.

Volpi, G., Magri, F., Frattini, P., Crosta, G. B. and Riva, F.: Groundwater-driven temperature changes at thermal springs in response to recent glaciation: Bormio hydrothermal system, Central Italian Alps, Hydrogeol. J., 25(7), 1967–1984, doi:10.1007/s10040-017-1600-6, 2017.

Whipp, D. M. and Ehlers, T. A.: Influence of groundwater flow on thermochronometer-derived exhumation rates in the central Nepalese Himalaya, Geology, 35(9), 851–854, doi:10.1130/G23788A.1, 2007.

Eigenständigkeitserklärung

Hiermit versichere ich, dass ich die vorliegende Arbeit selbstständig verfasst habe. Es wurden keine Quellen außer den ausdrücklich genannten verwendet. Wörtlich oder sinngemäß übernommenes Gedankengut wurde als solches kenntlich gemacht.

____________________________ ____________________________

Ort, Datum Unterschrift